Parcel Trajectories in Quasigeostrophic Jets: Neutral Modes*

LAWRENCE J. PRATT

Woods Hole Oceanographic Institution, Woods Hole, Massachusetts

M. SUSAN LOZIER

Ocean Sciences Program, Duke University, Durham, North Carolina

NATALIA BELIAKOVA

Woods Hole Oceanographic Institution, Woods Hole, Massachusetts

(Manuscript received 31 January 1994, in final form 4 November 1994)

ABSTRACT

The kinematics and dynamics of linear neutral modes propagating in a mean zonal jet are studied in an effort to understand how particle pathways within and across oceanic jets, such as the Gulf Stream, are determined. Sinuous-, varicose-, and mixed-mode waves are superposed on cusped jets that are governed by quasigeostrophic dynamics and characterized by piecewise uniform potential vorticity. Significant excursions (greater than the wave amplitude) of particle trajectories are found in the vicinity of steering lines that lie in the horizontal plane of motion, particularly when the background shear vanishes locally. Monochromatic waves produce pathways with simple periodic meandering, whereas a superposition of two waves results in chaotic parcel behavior, consistent with a number of earlier studies based on kinematic models. By identifying the steering surface, the surface on which the particle speed matches the speed of a propagating meander, as the site for preferential exchange, a mixing geometry associated with baroclinic oceanic fronts is suggested.

Flows containing a continuous distribution of normal modes (a wave packet) or of nonmodal disturbances are also studied. In the former case, chaos appears to be suppressed, and in the latter case, temporary disturbance amplification can lead to meridional exchange of fluid parcels.

1. Introduction

Over the past two decades, fluid pathways in the Gulf Stream have been traced by neutrally buoyant floats. The Lagrangian picture of the Gulf Stream that has emerged is markedly different from the familiar mean Eulerian description of a strong zonal jet extending essentially eastward. As seen in Fig. 1, the float pathways are marked by large-scale meandering with strong north–south excursions. Adding to the complexity of the trajectories are the smaller scales of motion that are superposed on the meandering. Additionally, trajectories are seen to track the warm and cold core rings spawned by the stream. Testimony to the strong temporal variability of the Gulf Stream, all of these motions so dominate the trajectories that the mean path of the stream is barely discernible.

The irregularity of these trajectories has raised the question as to what determines the pathway of water parcels within the Gulf Stream. Because these pathways are avenues of exchange for a suite of physical, chemical, and biological properties, an understanding of the mechanisms controlling them is essential to an understanding of property exchange across the Gulf Stream and other similar oceanic fronts. Because of their compelling size, it has commonly been thought that rings were the major contributor to the exchange of properties across the Gulf Stream. However, from an analysis of Gulf Stream '60 data, Bower et al. (1985) found that the contribution by rings to the total exchange of oxygen across the Gulf Stream was only 5%. This result shifted the focus of property exchange mechanisms away from rings to noncatastrophic events. Along this vein, Lozier and Riser (1990) demonstrated that exchange of potential vorticity across a midlatitude jet in a quasigeostrophic eddy-resolving general circulation model was accomplished via mixing mechanisms along simple meandering paths. Thus, the composite of trajectories shown in Fig. 1, and not just those exclusively linked to rings, are of interest for studies of property exchange.

* Woods Hole Oceanographic Institution Contribution No. 8659.

Corresponding author address: Dr. Lawrence J. Pratt, Department of Physical Oceanography, Woods Hole Oceanographic Institution, Woods Hole, MA 02543.

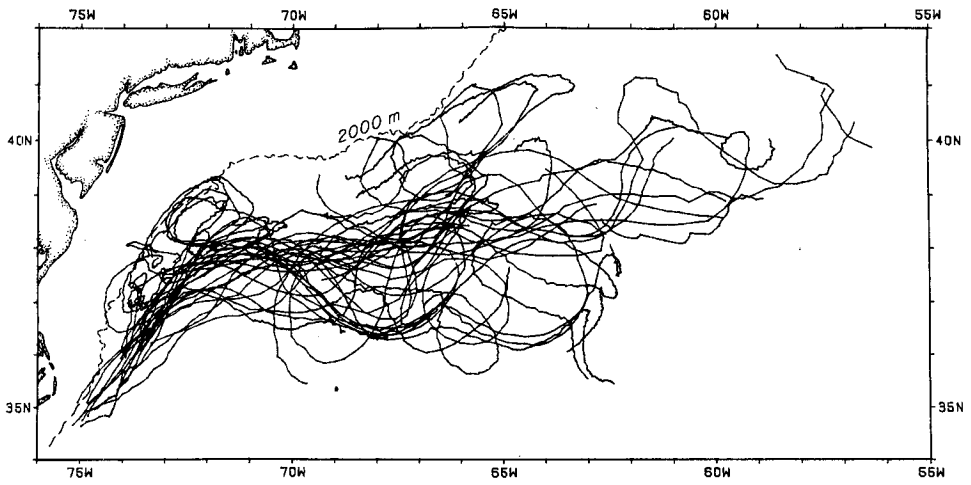

FIG. 1. Composite of Gulf Stream float trajectories (from Bower and Rossby 1989).

A number of recent calculations based on kinematic models of meandering jets have revealed striking Lagrangian properties. Bower (1991) has shown that the geometry of parcel motion in the crests and troughs of a steadily propagating meander depends crucially on whether the propagation is retrograde or prograde. Studies with two meanders of different frequency (e.g., Yang 1991; Dutkiewicz et al. 1993) or with a single meander of time-varying amplitude (Samelson 1992) suggest that parcel exchange between the core of the jet and eddies or trapped fluid in the flanges can occur. It is important to note that each of these studies relies on velocity fields that are kinematically plausible but not dynamically consistent. The fields are not solutions to the equations of motion and do not conserve potential vorticity; fluid parcels can move in chaotic ways without having to satisfy dynamical constraints. The constraint imposed by potential vorticity is seemingly fundamental to the understanding of fluid pathways in the Gulf Stream. A strong potential vorticity gradient separates the low potential vorticity waters of the Sargasso Sea from the high potential vorticity Slope waters. In a recent analysis of RAFOS float trajectories, Bower and Lozier (1994) conclude that the degree of float exchange across the Gulf Stream is highly dependent upon the existence and strength of the synoptic potential vorticity gradient. An interpretation of the float paths based on their kinematic characteristics alone was insufficient to predict the observed pathways. Based on these results, the need for dynamic constraints is clear.

Laboratory experiments with jets in annular geometries (Sommeria et al. 1989; Behringer et al. 1991) have focused on the potential vorticity gradient and its role as an inhibitor of mixing. Meandering jets produced by sources and sinks of fluid distributed around the annulus are characterized by a strong potential vorticity front situated at the jet axis. Experiments with dye injections revealed that this front is a barrier to mixing. These general features are verified by Behringer et al. (1991), who attempted to reconstruct the experimental trajectories by fitting an analytical form to the measured velocity field. Their calculated trajectories show limited regions of chaotic transport on the jet flanges, with the jet axis acting as a barrier.

To date only a few studies of parcel pathways in a jet have attempted to use dynamically consistent velocity fields; that is, fields that obey the potential vorticity equation to within some controllable approximation. Lozier and Bercovici (1992, hereafter abbreviated as LB) studied parcel exchange in the context of a baroclinically unstable, y-independent basic flow, $u(z)$. This study demonstrated the distinction between pathways at a steering level [where $u(z) = c_r$, the phase speed of the dominant wave] and those away from the steering level. It was shown that at a steering level parcels move unidirectionally northward or southward away from their initial position in an eastward-flowing jet. Away from the steering level the parcels oscillate in the ambient potential vorticity gradient. Lozier and Bercovici argued that although parcel behavior was explained with the kinematic properties u and c_r, it was the background potential vorticity gradient that controlled the location of the steering level.

Because of the lack of meridional structure in the model of LB, the steering level occurs at a constant elevation. However, in a jet with vertical *and* meridional variation a steering surface will result. The steering

surface, in general, will not coincide with a constant level of depth but rather will coincide with a selected isotach. Thus, in quasigeostrophic flow where the parcel motion is primarily horizontal, parcels will encounter steering lines and the steering effect will occur only at discrete values of y.

The role of meridional structure has been addressed by del-Castillo-Negrete and Morrison (1993) using wave fields that are dynamically consistent to within a linear approximation. Using a barotropic Bickley jet, trajectories are calculated using a velocity field consisting of the basic flow plus two linear neutral modes. With this system, del-Castillo-Negrete and Morrison investigate the conditions under which chaotic trajectories appear and make inferences about mixing based on these results. Also of relevance to our study are the dynamically consistent models of meandering jets explored by Garvine (1988) and Cushman-Roisin (1993; also see references contained therein). These studies concentrate on the sinuous-(meandering) mode parcel trajectories and the vertical motion produced as parcels move through crests and troughs of the meanders. Further remarks on these three references and their relevance to the present investigation follow in section 3.

The work we present generalizes the work of del-Castillo-Negrete and Morrison (1993) to include a simple form of baroclinicity and more general wave forms. The primary objective of our work is to determine the general characteristics of parcel trajectories throughout the jet and to understand how the ideas of parcel exchange developed by Lozier and Bercovici (1992) apply to a system with lateral shear. We expect fundamental differences when the plane of parcel motion no longer coincides with a steering surface. We explore these differences over a range of conditions. Specifically, we determine particle behavior in sinuous-, varicose-, and mixed-wave modes, distinguish between monochromatic waves and wave packets, address both modal and nonmodal disturbances, and examine parcel behavior in shear and local no-shear fields. Although the complexity of the Gulf Stream front warrants an investigation of pathways based on fully nonlinear and unstable wave dynamics, we cautiously approach this intractable limit by first investigating the pathways in linear, neutral wave fields superposed on a quasigeostrophic jet. The reasons for this simplification are twofold: First, we are able to find analytic solutions with these idealizations, and second, we believe that unscrambling the complexity of the fully nonlinear and unstable wave field will be aided by an understanding of a simpler system.

Additionally, we acknowledge that within linear wave fields potential vorticity is not exactly conserved. However, as with del-Castillo-Negrete and Morrison (1993), potential vorticity is conserved to within an approximation that depends on the ratio of wave amplitude to wavelength, a ratio that can be controlled. In contrast, potential vorticity is generally not conserved to *any* approximation in kinematic models. Our choice of quasigeostrophic dynamics for modeling strongly inertial jets is justified by numerous previous works that have demonstrated its ability to capture the essential features of observed jets, such as the Gulf Stream.

In section 2 the kinematic considerations of flow in the vicinity of steering lines is developed. Section 3 details studies of monochromatic waves superposed on a piecewise-uniform potential vorticity jet, with the extension to wave packets covered in section 4. For completion, the behavior of pathways due to nonmodal disturbances (the continuous spectrum) is explored in section 5. A summary is given in section 6.

2. General considerations

a. *Trajectory equations, steering surfaces, and steering lines*

Consider a zonal, quasigeostrophic jet with dimensionless eastward velocity $U(y, z)$. Small disturbances to the basic streamfunction of the form $\mathrm{Re}[\Phi(y, z)e^{ik(x-ct)}]$ obey

$$(U-c)\left[\frac{\partial}{\partial z}\left(\frac{1}{S}\frac{\partial \Phi}{\partial z}\right)+\frac{\partial^2\Phi}{\partial y^2}-k^2\Phi\right] + \left[\beta-\frac{\partial^2 U}{\partial y^2}-\frac{\partial}{\partial z}\left(\frac{1}{S}\frac{\partial U}{\partial z}\right)\right]\Phi = 0 \quad (2.1)$$

(Pedlosky 1979), where $S = (N^2D^2)/(f_0^2L^2)$ and $\beta = \beta_0 L^2/U$ and the remaining notation and nondimensionalization are standard. The flow is confined between the upper surface $z = z_T$ and bottom $z = \eta_B(y)$, and the corresponding linearized boundary conditions are

$$(U-c)\frac{\partial \Phi}{\partial z}+\left[S\frac{\partial \eta_B}{\partial y}-\frac{\partial U}{\partial z}\right]\Phi = 0 \quad (z=0) \quad (2.2)$$

and

$$(U-c)\frac{\partial \Phi}{\partial z}-\frac{\partial U}{\partial z}\Phi = 0 \quad (z=z_T). \quad (2.3)$$

In addition, the jet lies within a channel having vertical walls at $y = \pm w$, where w may be infinite. The corresponding boundary conditions are

$$\Phi(\pm w, z) = 0. \quad (2.4)$$

Quasigeostrophic theory assumes that the slopes of isopycnal surfaces and of top- and bottom-boundary surfaces are vanishing small. As a consequence, the motion of fluid parcels is approximately horizontal and quasigeostrophic potential vorticity is conserved following the horizontal geostrophic velocity. To remain consistent, fluid trajectories must be calculated on the basis of the horizontal velocity; accounting for the small vertical velocity would result in departures of negligible

importance. For a fluid parcel with Lagrangian coordinates (X, Y) moving on a plane, z = const, the trajectory is determined by

$$\frac{dX}{dt} = U(Y, z) - \frac{\partial \phi}{\partial Y}(X, Y, z, t) \quad (2.5a)$$

and

$$\frac{dY}{dt} = \frac{\partial \phi}{\partial X}(X, Y, z, t), \quad (2.5b)$$

where ϕ is the perturbation streamfunction for the full (nonlinear) disturbance field. For small-amplitude wave motion, ϕ is expanded in integer powers of a (a is a measure of the wave amplitude), the leading order contribution of which is $a\,\mathrm{Re}[\Phi e^{ik(x-ct)}]$. The temptation to expand Y similarly should be resisted as northward parcel excursions much larger than the wave amplitude are possible, as will be shown later.

Although the wave phase speed c may be complex, the goal of the present discussion is to analyze the case of neutral waves (real c). We will begin by analyzing the case of a monochromatic neutral wave with the form $\phi = a\Phi(y, z)\cos k(x - ct)$ and later consider sums of such waves (or corresponding Fourier integrals). For a single wave, it is convenient to view the motion in a frame of reference moving with speed c, so that the flow appears steady. Defining $X_m = X - ct$ and substituting the expansion for ϕ into (2.5a,b) leads to

$$\frac{dX_m}{dt} = U(Y, z) - c + 0(a) \quad (2.6a)$$

and

$$\frac{dY}{dt} = -ka\Phi(Y, z)\sin kX_m + 0(a^2). \quad (2.6b)$$

In the model of LB, where U is y independent, the wave modes are not constrained to satisfy any lateral boundary condition and therefore ϕ is y independent. Therefore, at the steering level [the depth, z, where $U(z) = c$], X_m remains fixed, and according to (2.6b), $|Y|$ grows linearly with time. The parcels therefore execute straight trajectories and move off to $y = \pm\infty$ (according to the sign of $\sin kX_m$). Although there is no meridional structure to define a jet, the cross-stream motion implies the potential for parcel exchange. Thus, parcel exchange is confined to the steering level because at all other levels X_m varies linearly with time such that Y is periodic.

To what extent do the results of LB apply when $\partial U/\partial y \neq 0$? Although determination of Φ in such cases is nontrivial, we may learn a great deal about the resulting trajectories from (2.6a,b) for rather general Φ. To begin with, we observe that the fixed points (zeros of the right hand sides) occur where

$$U(y, z) = c \quad (2.7)$$

and

$$kX_m = n\pi \quad (n = 0, \pm 1, \pm 2, \cdots). \quad (2.8)$$

According to (2.7), the fixed points occur on a steering *surface* $z = z_s(y)$. As shown in Fig. 2, intersections between the steering surface and horizontal planes $z = z_0$ occur along one or more steering *lines* $y = y_s$. For example, the basic velocity $U_0 = e^{-y^2-z^2}$ has steering surfaces consisting of circular cylinders, $y^2 + z^2 =$ constant. For a wave having $c > 0$, the steering lines at level z_0 are given by $e^{-y_s^2-z_0^2} = c$. Fixed points occur along the steering lines at the spacing π/k, corresponding to the locations of crests and troughs of the wave.

Since the parcel motion is horizontal to lowest order, determination of the trajectories is similar to that for a z-independent flow. We simply treat z as a parameter in (2.6) and analyze the solutions near the fixed points. The structure of the trajectories near such points has previously been discussed in barotropic models (e.g., del-Castillo-Negrete et al. 1993). In the next section we review and augment that discussion and explore an exceptional case that arises when a steering line occurs at a point of grazing contact between the steering surface and the horizontal plane in question (at z_{00}, $y = 0$ in Fig. 2).

b. *Trajectories for the case $\partial U/\partial y \neq 0$ at $y = y_s$*

To determine the qualitative behavior of a parcel in the vicinity of a fixed point $(X_m = n\pi/k, Y = y_s)$, let $\xi = (X_m - n\pi/k)$, $\eta = (Y - y_s)$, and assume that $|\xi| \ll 1$ and $|\eta| \ll 1$. Substitution into (2.6a,b) leads to

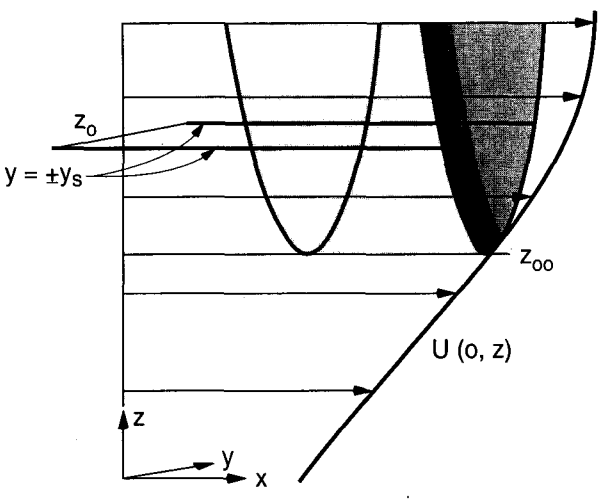

FIG. 2. Definition sketch showing a steering surface and steering lines in a jet with horizontally and vertically decaying velocity. A vertical section of the velocity profile $U(y, z)$ is shown at $y = 0$. We imagine that the velocity also decays with increasing $|y|$ (not shown). The parabolic lines coincide with the steering surface $U(y, z) = c$, which intersects the plane $z = z_0$ along the steering lines $y = \pm y_s$. The steering surface extends only to the elevation z_{00}.

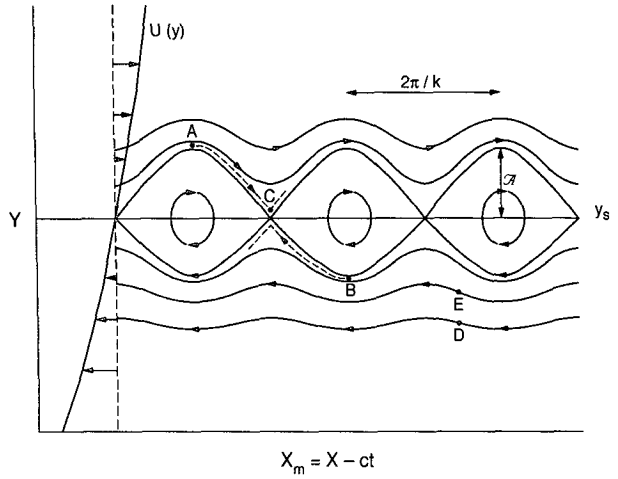

FIG. 3. Schematic sketch showing parcel trajectories near a steering line in horizontal section. The arrows indicate the basic shear, which is nonzero at the steering line. The trajectories are shown in a frame of reference moving with the wave.

$$\frac{d\xi}{dt} = \eta \frac{\partial U}{\partial y_s} \tag{2.9a}$$

and

$$\frac{d\eta}{dt} = -(-1)^n k^2 \Phi(y_s, z)\xi, \tag{2.9b}$$

where $\partial U/\partial y_s$ denotes $(\partial U/\partial y)_{y=y_s}$. It will be shown shortly that $\eta = 0(a^{1/2})$ so that the previously neglected $0(a)$ terms in (2.9a) are, in fact, negligible.

Substitution of the solution $\xi = Ae^{\sigma t}$ and $\eta = Be^{\sigma t}$ into (2.9a,b) leads to

$$\sigma^2 = -(-1)^n a k^2 \Phi(y_s, z)(\partial U/\partial y_s). \tag{2.10}$$

The fixed points are unstable when σ is real and stable when σ is imaginary. In the former case there are converging and diverging trajectories from the fixed points, and in the latter, the trajectories form closed orbits about the fixed points.

As will be shown in later sections, the stable and unstable fixed points are generally centered in a heteroclinic "cat's eyes" pattern. A qualitative representation for the case in which $\partial U/\partial y_s > 0$ is shown in Fig. 3. In interpreting this and later trajectory diagrams, it is important to remember that the closed curves forming the cat's eyes are an artifact of the moving-coordinate system. Plots of the corresponding parcel paths in a rest frame would yield open curves. Nevertheless, Fig. 3 describes the novel feature of trajectories near a steering line: parcels having relatively large separations in y can be brought into close proximity. For example, parcels originating at A and B will come into close contact when they are near the unstable node C, whereas the parcels originating at D and E maintain roughly the same y separation. The implications for parcel exchange are therefore clear; if slight deviations from the base trajectories occur near the unstable node, the parcel may be diverted to an entirely different path and may be carried large meridional distances from its undisturbed path. The deviations may be caused by nonconservative processes such as diffusion (Dutkiewicz et al. 1993) or by secondary waves (del-Castillo-Negrete et al. 1993; Behringer et al. 1991). (An example of the latter is given in section 3.) These studies suggest that the extent of mixing is sensitive to the particular mode interaction or diffusion present. Alone, the trajectories of Fig. 3 show no parcel exchange, and this distinguishes the result from that of LB. The meridional gradient of U ensures a nonzero $U - c$ along the trajectory, and thus the unidirectional meridional movement noted by LB is inhibited.

Since the unstable fixed points provide possible centers of parcel exchange, it is worth understanding the associated kinematics on physical grounds. Suppose that $\Phi(y_s, z)$ is positive at a particular z, so that the perturbation pressure, $a\Phi(y_s, z)\cos kX_m$, is positive at the fixed points $X_m = n\pi/k$ (n even) and negative for odd n. Consider the point $n = 1$, which has negative perturbation pressure and is therefore associated with cyclonic perturbation (or wave) vorticity. Referring to Fig. 4, a parcel originating at point P_1 to the northeast of the fixed point will tend to move northward due to the anomalous positive vorticity. As it moves a distance η_1' northward, it is advected a distance ξ_1' eastward by the basic velocity. Subsequent northward displacement (η_2') moves the parcel into latitudes of even stronger eastward basic flow, and the parcel is carried away at an increasing rate. A similar effect takes place in quadrant 3, this time with motion toward the southwest. (Again the reader is reminded that "east" and "west"

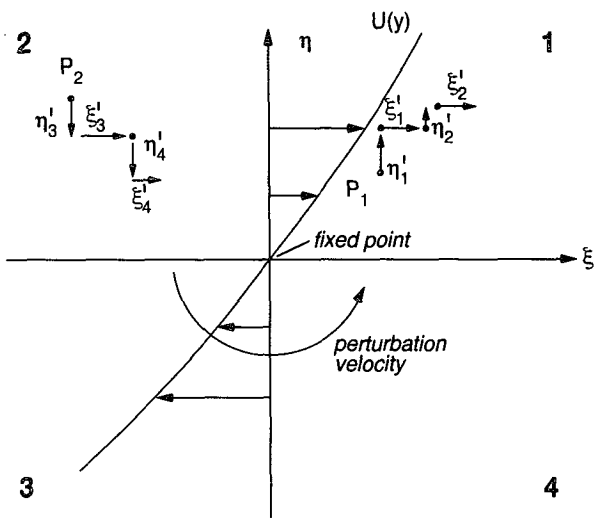

FIG. 4. Schematic sketch showing the direction of parcel motion in quadrants 1 and 2 in the vicinity of a fixed point with finite shear.

are directed relative to our moving frame.) In quadrants 2 and 4, basic advection and perturbation vorticity combine to bring parcels closer to the fixed point. At point P_2, for example, the southward motion of the parcel, induced by the cyclonic vorticity, is accompanied by eastward advection.

In general, the pattern of outward movement in two opposing quadrants accompanied by inward movement in the remaining two quadrants arises whenever the vorticity anomaly due to the wave opposes the basic vorticity. When the two vorticities agree in sign, the parcels orbit the fixed point, as can be shown by similar arguments. Equation (2.10) is simply a mathematical justification of these physical arguments, the right-hand side being positive when the sign of the pressure anomaly $[(-1)^n a\Phi]$ opposes the sign of the basic shear $\partial U/\partial y_s$.

The width of the cat's eyes pattern (twice the distance A in Fig. 3) can be estimated from (2.6a) and (2.6b). Dividing the latter by the former results in

$$\frac{dY}{dX_m} = \frac{-ka\Phi(Y, z)\sin kX_m}{U(Y, z) - c}. \tag{2.11}$$

In the case that the cat's eyes width is much less than the scale of y variation of U and Φ, we may approximate Φ by $\Phi(y_s, z)$ and $U - c$ by the leading term in its Taylor expansion about Y_s, namely $Y(\partial U/\partial y_s)$. Integration of (2.11) from an unstable node to a point $\pi/2k$ downstream yields

$$A \approx \left[\frac{2a\Phi(y_s, z)}{(\partial U/\partial y)_{y=y_s}}\right]^{1/2}. \tag{2.12}$$

It is important to note that $A \sim a^{1/2}$, so that linear waves ($a \ll 1$) create cat's eye patterns (and possible parcel exchange) over much greater meridional extent than the streamline displacements. As the local meridional shear $\partial U/\partial y_s$ decreases, A increases, and the meridional band occupied by the cat's eyes grows. As $dU/dy_s \to 0$ (over the entire domain), the cat's eyes fill the entire plane, and the (moving frame) trajectories become aligned north and south, as in LB.

c. *Trajectories for the case $\partial U/\partial y = 0$ at $y = y_s$*

When $\partial U/\partial y = 0$ at the fixed point, the arguments of the previous section must be altered. One must now consider the small changes in U due to the curvature U_{yy}, so that (2.9a) is replaced by

$$\frac{d\xi}{dt} = \frac{1}{2}\eta^2\frac{\partial^2 U}{\partial y_s^2}. \tag{2.13}$$

[We show later that $\eta^2 = 0(a^{2/3})$, so that the neglect of higher-order terms in the wave amplitude is consistent.] If (2.13) is multiplied by $\xi/(\partial^2 U/\partial y_s^2)$ and (2.9b) by $\eta^2/3(-1)^n ak^2\Phi(y_s, z)$ and the two results are subtracted, we find

$$\eta = \left[c_0 - \frac{3(-1)^n ak^2\Phi(y_s, z)\xi^2}{\partial^2 U/\partial y_s^2}\right]^{1/3}, \tag{2.14}$$

where c_0 is a constant. The trajectories for this case form upward and downward cusps at the fixed points, as shown in Fig. 5 for the case $\partial^2 U/\partial y_s^2 > 0$ (changing the sign of $\partial^2 U/\partial y_s^2$ merely changes upward pointing cusps to downward-pointing cusps, and vice versa).

The width of the meridional band of cusps (the distance A' in Fig. 5) can be estimated by approximating $U - c$ as $\frac{1}{2}Y^2\partial^2 U/\partial y_s^2$ in (2.11) and repeating the procedure used to obtain the cat's eyes width. The result,

$$A' \approx \left[\frac{6a\Phi(y_s, z)}{\partial^2 U/\partial y_s^2}\right]^{1/3}, \tag{2.15}$$

shows that the meridional extent of the cusped trajectories is now $0(a^{1/3})$ and therefore greater than the case of finite horizontal shear. Despite this increase in amplitude, the potential for mixing in this case of zero local shear is possibly diminished from the case with nonzero local shear. This is due to the difference in the geometry of the trajectory patterns. As seen from Fig. 5, trajectories that are bringing waters from north of the steering line are displaced one-half of a wavelength from those bringing waters from south of the steering line. This contrasts with the situation for local shear, where the convergent trajectories approach the steering line at the same place, thus bringing waters across the jet into closer proximity.

d. *Conditions for the existence of steering lines*

According to (2.1), the condition $U - c = 0$ can occur only in special circumstances for neutral modes. [Corresponding restrictions occur in the boundary conditions (2.2) and (2.3) if $U - c = 0$ at the upper or lower boundary.] If the perturbation potential vorticity $\partial(S^{-1}\partial\Phi/\partial z)/\partial z + \partial^2\Phi/\partial y^2 - k^2\Phi$ is nonsingular at the steering line, then the expression $(\partial Q/\partial y)\Phi\{= [\beta - \partial^2 U/\partial y^2 - \partial/\partial z(S^{-1}\partial U/\partial z)]\Phi\}$, must vanish there. (Here Q is the potential vorticity of the unperturbed flow field.) To meet the latter condition, it is possible that $\Phi(y_s, z)$ could vanish; however, that would be tantamount to having a rigid wall with no

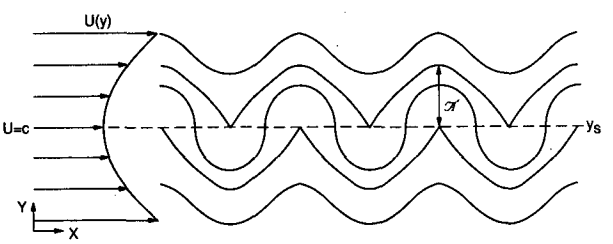

FIG. 5. Moving-frame trajectories near a steering line with zero shear but finite shear curvature.

normal velocity at the steering line, and no cat's eye patterns would exist there. Even if such modes occurred, they would be of no interest from the standpoint of parcel exchange. The more relevant situation would be that $\partial Q/\partial y$ vanish, and we now discuss the likelihood of this circumstance in more detail.

In barotropic flows, $\partial Q/\partial y$ may vanish at one or more values of y, corresponding to one or more values of U. If the basic flow has continuously varying Q and reasonably simple structure, $\partial Q/\partial y$ will vanish at just a few values of U, and possible neutral wave phase speeds will be limited to these U values. Thus, the number of neutral waves with steering lines (and with $\Phi \neq 0$ at the steering lines) is very restricted. An exception occurs when Q is piecewise uniform, and we give some examples in the next section.

For the case of baroclinic flow, in which the positions of the steering lines vary with z, the situation is even more restrictive. In order for a steering surface with nonzero Φ to exist, the conditions $\partial Q/\partial y = 0$ and U = constant must hold at all locations on this surface. Although it is possible to contrive a basic flow with this property (Charney and Stern 1962), it is better to appeal to some physical process that might predispose the basic flow to have this configuration. It is plausible that critical-layer processes brought into play by a forced wave would homogenize the potential vorticity along a surface of U = constant. Haynes (1989) and Haynes and McIntyre (1987) have demonstrated that this process can act in a barotropic flow, and it is possible that corresponding processes could take place in baroclinic flows.

The third condition allowing $U - c = 0$ in (2.1), (2.2), and (2.3) is that the perturbation potential vorticity is singular, as occurs in the continuous spectrum. This case is discussed further in section 5.

3. Examples of trajectories for monochromatic waves

Having focused to this point on the kinematics associated with steering lines that intersect planes of particle motion, we now investigate particle trajectories from dynamically consistent flow fields. Because of their analytical tractability, we have chosen to use mean flows with piecewise-uniform potential vorticity. These jets are able to support neutral modes having meridional structures that can be described as sinuous (leading to a meandering behavior), symmetrical (leading to a varicose behavior), or mixed (containing elements of both). In this section we compute examples of trajectories for waves of each type.

a. Sinuous Mode

The cusped jet of Pratt and Stern (1986), which arises in an equivalent barotropic (or 1½ layer) model, serves as a simple starting point for our examples. The potential vorticity in the active layer is assumed to be piecewise uniform, having (nondimensional) value q_0 to the south of the line $y = 0$ and $q_0 + 1$ to the north, and the basic velocity is

$$U(y) = e^{-|y|}. \tag{3.1}$$

This jet is linearly stable, and the normal modes are described by the disturbance streamfunction

$$\phi = ae^{-\kappa|y|}\cos k(x - ct), \tag{3.2}$$

where

$$c = 1 - (1 + k^2)^{-1/2}, \tag{3.3a}$$

and

$$\kappa = (1 + k^2)^{1/2}, \tag{3.3b}$$

where a and k are the wave amplitude (assumed $\ll 1$) and wavenumber, respectively.

The trajectory equations for the flow are

$$\frac{dX_m}{dt} = e^{-|Y|} - c \tag{3.4a}$$

and

$$\frac{dY}{dt} = -kae^{-\kappa|Y|}\sin kX_m. \tag{3.4b}$$

According to (3.1), the cusped jet has a velocity profile that decays to the north and south of the centerline ($y = 0$) over the Rossby radius of deformation (= 1 in the current nondimensional units). When the potential vorticity front forming the jet centerline is disturbed, vorticity anomalies are set up, leading to a restoring effect similar to that which acts in an ordinary Rossby wave. The disturbances decay meridionally over a scale κ^{-1}. The decay is symmetric about the jet axis, as is the corresponding meridional velocity. The disturbance may therefore be classified as sinuous. According to (3.3a), the phase speed ranges from zero (for long waves) to unity (for short waves), which is also the range of variation of the basic velocity. For this jet then, steering lines exist for all waves because at each steering line the condition $\partial Q/\partial y = 0$ is obviously satisfied. The only y that cannot be a steering line is the centerline ($y = 0$) of the jet, where $\partial Q/\partial y$ is essentially infinite. This exclusion is consistent with the fact that jet centers have been described as barriers to parcel exchange both experimentally (Behringer et al. 1991; Sommeria et al. 1989) and observationally (Bower and Lozier 1994).

Figure 6a shows the trajectory field for the wave $k = 1$ and $a = 0.01$, which has steering lines at $y_s \approx \pm 1.23$. Characteristic of sinuous modes, the two rows of cat's eyes are 180° out of phase. Note that the amplitude of the wiggles of the centerline trajectory, which we anticipate to be $0(a)$, are in fact considerably smaller than the amplitude of the wiggles

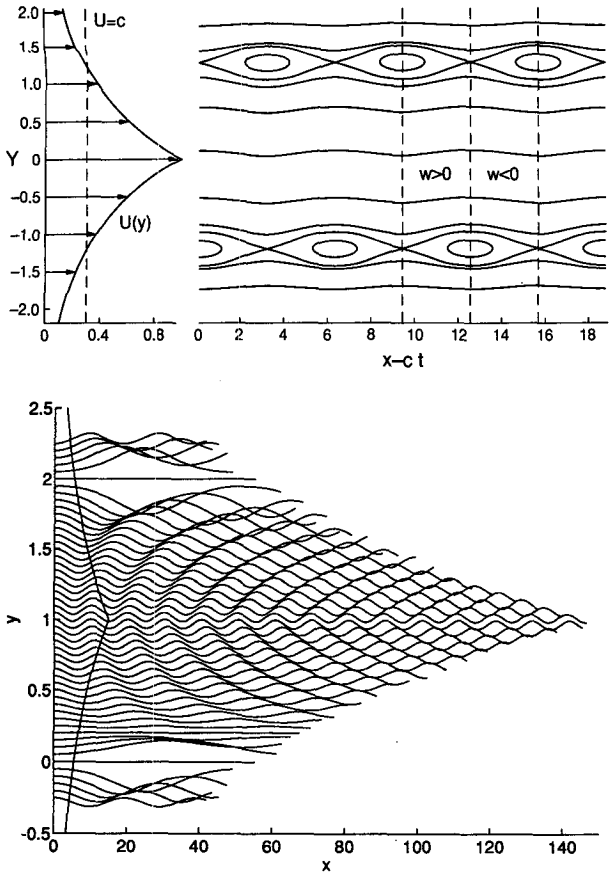

FIG. 6. (a) Moving-frame trajectories for a sinuous wave in $-|y|$ a cusped jet: $U(y) = e$, $k = 1$, $a = 0.01$, and $c = 0.29$. (b) Fixed-frame trajectories for a raft of floats launched at $y = 0$ for $t = 0$ with the wave given in (a). The total elapsed time $t = 150$ is the same for each trajectory.

of the trajectories bordering the cat's eyes, anticipated to be $0(a^{1/2})$.

Figure 6b shows the trajectories executed by a number of floats launched over a range of latitudes. The results were obtained using a Matlab fourth-order Runge-Kutta scheme, with an error tolerance of 10^{-9}. The float trajectories are plotted in a rest frame (X rather than X_m), so that no closed orbits exist. All float paths were computed over a set time interval, and therefore, because of the velocity shear, the distance traveled in that time differs with latitude. The pattern created by the differing float pathlengths is simply a reflection of the velocity pattern. Paths also differ in terms of wavelength and amplitude. Floats launched near the centerline are characterized by smaller amplitudes and shorter wavelengths, with the former due to the fact that the more rapidly moving floats are able to overtake and pass through more waves in a given time. Due to the symmetry of the jet, any two floats launched at equal but opposite distances from the steering lines have trajectories with identical wavelengths, yet they are out of phase. The maximum amplitude is reached near the steering line.

When floats are launched near or within the cat's eyes, the details of the motion are sensitive to small departures from the monochromatic trajectory field. As a demonstration, we add to the Fig. 6a wave a secondary wave of smaller amplitude and length. Figures 7a–c show the trajectories of parcels launched at $\Delta y = 0.005$ and $\Delta x = 0.0015$ to the northeast of one of the southern saddle points. The second wave has a wavenumber $k = 2$ and corresponding amplitudes of 10^{-5}, 10^{-4}, and 10^{-3}, for Figs. 7a,b,c, respectively. As the secondary wave amplitude is increased, the trajectories begin to cross the critical line ($y \approx -1.25$) and take on increasingly irregular appearances.

In their study of neutral waves of the Bickley jet, del-Castillo-Negrete and Morrison (1993) show that chaos is generally restricted to the region near the critical line, provided that the wave amplitudes are small. For a superposition of two neutral waves, chaotic regions will lie about the critical lines of each wave and will be separated from each other by bands of regular trajectories. If the wave amplitudes are increased beyond infinitesimal levels, the regular bands, which act as barriers, begin to disappear, eventually resulting in a phenomenon known as resonance overlap.

Another phenomenon that can broaden the area of chaos is seperatrix reconnection, in which the amplitude of one wave is sufficiently large that seperatricies from different critical lines of that wave become attached. Although our solutions display resonance overlap and separatrix reconnection, we caution that both usually require amplitudes larger than those that can be substantiated by a linear approximation. Although some fully nonlinear solutions exist exhibiting Lagrangian chaos in simple vortex structures (e.g., Polvani and Wisdom 1990) none apparently have been found for meandering jets.

We also note that fluid parcels do undergo weak vertical excursions. At the interface separating upper and lower fluids, for example, the vertical velocity is

$$w = -\epsilon \frac{d\phi}{dt} = -\epsilon akce^{-\kappa|y|} \sin k(x - ct),$$

where ϵ is the vanishingly small Rossby number. In our frontal model, where meander crests lie at $k(x - ct) = n\pi$, downwelling occurs to the right of crests and to the left of troughs, or what is sometimes referred to as the front side of the meander. Upwelling occurs on the "back side" of the meander, to the left of crests and to the right of troughs. For any fixed x, the vertical velocity has the same sign to the north or south of the front. These patterns, which are indicated in Fig. 6a, are consistent with the upwelling

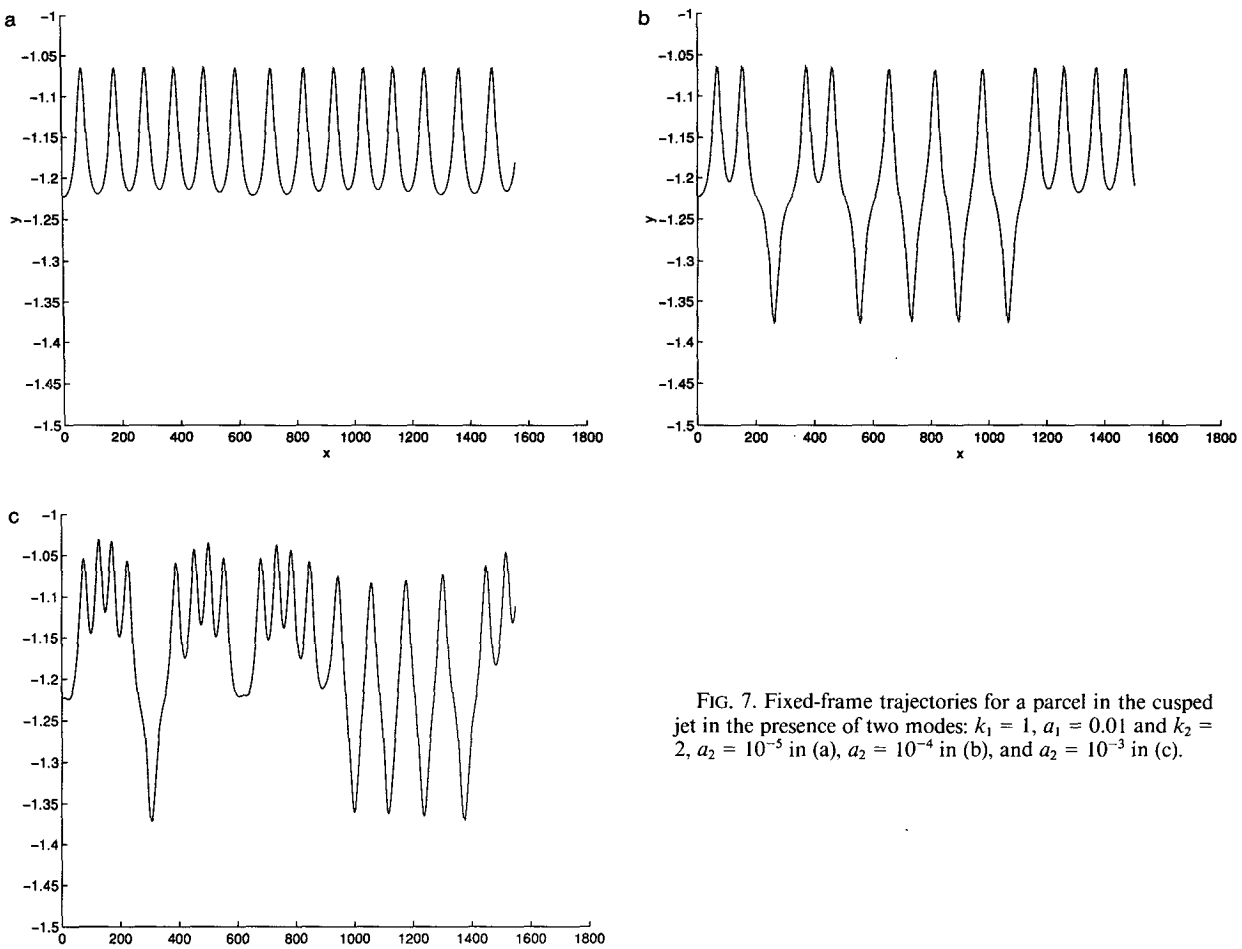

FIG. 7. Fixed-frame trajectories for a parcel in the cusped jet in the presence of two modes: $k_1 = 1$, $a_1 = 0.01$ and $k_2 = 2$, $a_2 = 10^{-5}$ in (a), $a_2 = 10^{-4}$ in (b), and $a_2 = 10^{-3}$ in (c).

patterns computed in models due to Garvine (1988) and Cushman-Roisin (1993) and with Gulf Stream observations by Bower and Rossby (1989). In non-quasigeostrophic models where the vertical velocity could be large enough to influence horizontal trajectories by moving parcels in a vertically sheared horizontal velocity field, the general character of the chaos might be considerably different than the picture presented here.

b. *Varicose mode*

Adding a second potential vorticity front gives the model considered in (3.1) an extra degree of freedom, allowing two meridional modes for each k. The basic velocity,

$$U(y) = [e^{-|y-L_1|} - re^{-|y-L_2|}], \tag{3.5}$$

has cusps at two potential vorticity fronts, $y = L_1$ and $y = L_2$, with $L_1 > L_2$. The parameter $-r$ is the ratio of the potential vorticity change across $y = L_2$ to the change across $y = L_1$. The wave-amplitude function is given by

$$a\Phi(y) = a\begin{cases} e^{-\kappa(y-L_1)} & (y > L_1) \\ (1 - be^{-\kappa\Delta L})e^{\kappa(y-L_1)} + be^{-\kappa(y-L_2)} & \\ \qquad\qquad (L_2 < y < L_1) & \\ [(1 - be^{-\kappa\Delta L})e^{-\kappa\Delta L} + b]e^{\kappa(y-L_2)} & \\ \qquad\qquad (y < L_2), & \end{cases} \tag{3.6}$$

where

$$b = e^{\kappa\Delta L}[1 + \kappa(c - 1 + re^{-\Delta L})^{-1}],$$
$$\Delta L = L_1 - L_2,$$

and c is determined by

$$(c)^2 - (1 - r)(e^{-\Delta L} + 1 - \kappa^{-1})c - \kappa^{-1}(e^{-\Delta L} - r) + (1 - re^{-\Delta L})(e^{-\Delta L} - r + r\kappa^{-1}) - r\kappa^{-2}(1 - e^{-2\kappa\Delta L}) = 0. \tag{3.7}$$

The derivation of these results and additional details can be found in Pratt et al. (1991).[1]

[1] Readers who wish to investigate Pratt et al. (1991) should note that the variables $2c$, $2U$, l_o, a, and A in that reference should be replaced by the present variables c, U, κ, b, and a, respectively.

We can investigate a variety of stable and unstable, symmetrical and asymmetrical jets by varying the parameter r. The flow is stable for $r < 0$, and the corresponding neutral waves all have steering levels, as before. First consider the case $r = -1$, for which the basic velocity $U(y) = [e^{-|y-L_1|} + e^{-|y-L_2|}]$ is distributed symmetrically about the line $y = (L_1 + L_2)/2$, as shown in Fig. 8a. The phase speed for this case is given by

$$c = e^{-\Delta L} + 1 - \kappa^{-1} \pm \kappa^{-1} e^{-\kappa \Delta L}, \qquad (3.8)$$

where "+" indicates a varicose mode and "−" a symmetric mode. The amplitude function for the former case is

$$a\Phi(y) = a \begin{cases} e^{-\kappa(y-L_1)} \\ [\pm e^{-\kappa(y-L_2)} - e^{\kappa(y-L_1)}]/[\pm e^{-\kappa \Delta L} - 1] \\ [-e^{-\kappa \Delta L} \pm 1] e^{\kappa(y-L_2)}/[\pm e^{-\kappa \Delta L} - 1]. \end{cases} \qquad (3.9)$$

Varicose modes have c ranging from $e^{-2\Delta L}$ to $e^{-\Delta L} + 1$, whereas $U(y)$ ranges from 0 to $e^{-\Delta L} + 1$, so that all waves have steering lines but each value of y is not necessarily a steering line.

A peculiarity of the case $r = -1$ is that the basic velocity profile has a relative minimum at the centerline and maxima at $y = L_1, L_2$. As c is varied, it is therefore possible for two to four steering lines to occur, depending on whether c is less than, equal to, or greater than the centerline value of U. The first possibility is the most natural, as geophysical jets generally have one velocity maximum and therefore at most two steering lines. The case of three steering lines is less likely but extremely interesting as the basic shear vanishes at the middle steering line (the exceptional case discussed in section 2c). We will therefore present one example having two steering lines and one with three steering lines. The case of four steering lines will be skipped.

Figure 8a shows the trajectories for a varicose wave with $k = 1$ and $a = 0.01$. In contrast to the sinuous mode (Fig. 6a), the two rows of cat's eyes are in phase, and the centerline trajectory is straight. Figure 8b shows the trajectories for a raft of floats launched at various values of y in the varicose wave field. As before, floats launched near the cat's eyes may execute irregular trajectories, provided that some additional time dependence or noise is introduced.

The interfacial vertical velocity for the varicose mode is

$$\omega = -\epsilon akc\{+\} \sin k(x - ct),$$

where $\{+\}$ is the expression in (3.9) evaluated using the "+" sign. As labeled in Fig. 8a, w reverses sign on either side of the centerline of the flow. To the north of the centerline, upwelling occurs to the left of cat's eyes and right of saddle points (corresponding to the left of troughs and right of crests of the north front). Downwelling occurs to the right of cat's eyes and left of the saddle points. To the south of the centerline the pattern is reversed.

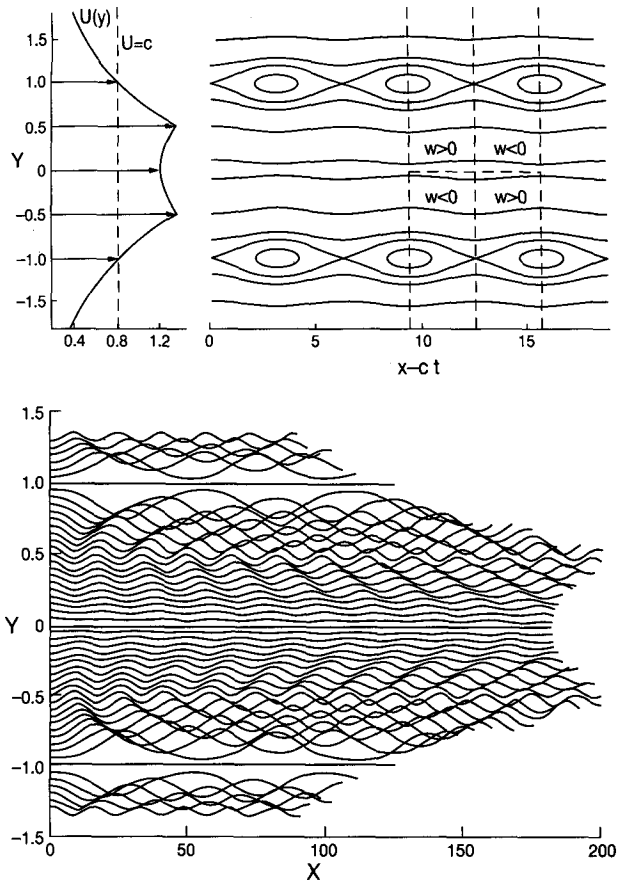

FIG. 8. (a) Moving-frame trajectories for a varicose mode in a jet with a double cusp (and $r = -1$). The wave is given by $k = 1$, $a = 0.01$, $c = 0.8326$. (b) Fixed-frame trajectories for a raft of floats launched at $y = 0$ for $t = 0$ in the wave field of (a). The total elapsed time, $t = 150$, is the same for each trajectory.

Sinuous modes with two steering lines can also be found for the case $r = -1$. However, the trajectory patterns are qualitatively the same as those of the single cusped jet (Fig. 6a). The sinuous mode does play an important role in the discussion of the case of three steering lines, which follows next.

c. *Sinuous and varicose modes for the case $dU/dy_s = 0$*

It is possible to fix k such that $U = c$ at the centerline latitude of the jet, where $dU/dy = 0$. For a varicose wave, in which v is symmetric about the centerline, there is no meridional motion there and the nearby trajectories are parallel, east–west lines. [Since $\Phi(y_s) = 0$ for this case, the cat's eye width A' is zero in (2.14).] The trajectory field for this case is qualitatively the same as in Fig. 8a.

A more interesting situation arises when the wave has three steering levels and a sinuous structure. Here

the "−" sign must be used in (3.7) and (3.8) to obtain the dispersion relation and amplitude function. According to (3.7), c ranges over zero to $e^{-\Delta L}+1$, which is also the range of variation of $U(y)$. Choosing $k=0.3$ and $\Delta L=1$ gives a wave with steering levels at $y\approx\pm 0.6$ and $y=0$. In contrast with the varicose wave case, the meridional velocity is finite at $y=0$, and cusps form at the corresponding critical points as shown in Fig. 9. The wave amplitude a is 0.01 for this case. Notice that the trajectories near the cusps execute somewhat larger meridional excursions than those near the cat's eyes, a consequence of the $a^{1/3}$ width scale. Unlike the case with cat's eyes, however, all trajectories are contiguous and do not appear to offer the same opportunity for exchange.

d. Mixed mode

When $-1<r<0$, the basic velocity is asymmetric and pure varicose and sinuous modes no longer exist. (The Gulf Stream is an example of an asymmetric flow, with the cyclonic shear stronger than the anticyclonic shear.) For flow with two steering lines, the cat's eyes become phase shifted by an amount $0<\Theta<\pi$. An example appears in Fig. 10 for the case $r=0.2$, $k=1.8$, $a=0.01$. Note that the cat's eyes near $y=0$ are larger than those near $y=2$.

4. Parcel motion in wave packets

Although our discussion has centered on monochromatic and two-wave perturbations, in practice, disturbances will consist of a superposition of waves of different lengths from the discrete and continuous spectrums. We will reserve discussion of the latter for the next section. For the present, consider the parcel motion due to a Fourier superposition of neutral waves:

$$\phi(x,y,z,t)=\frac{1}{\sqrt{2\pi}}\int_{-\infty}^{\infty}F(k,z,y)\times\cos[kx-\omega t+\theta(k)]dk.$$

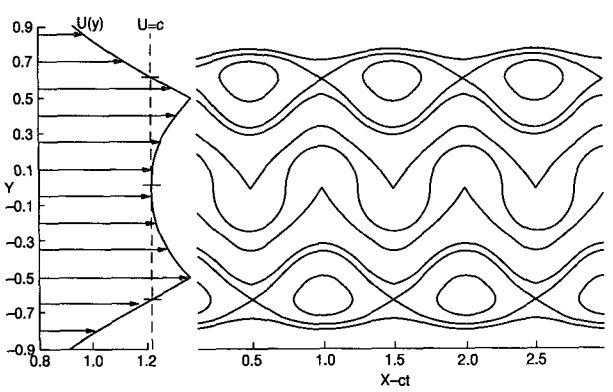

FIG. 9. Moving-frame trajectories for a sinuous mode ($k\approx 6.39$, $a=0.01$, $c=1.21$) in the double-cusp jet with $r=-1$.

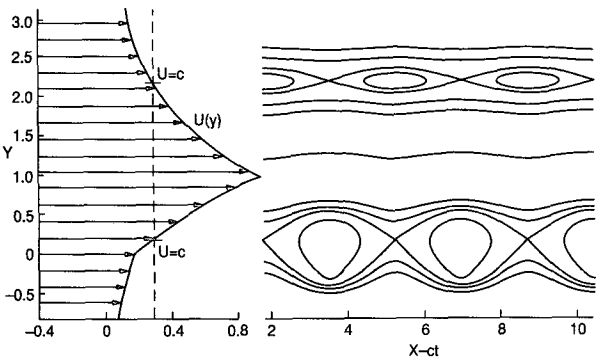

FIG. 10. Moving-frame trajectories in an asymmetric jet ($r=0.2$) with a mixed neutral mode ($k=1$, $a=0.01$, $c\approx 0.27$).

Using standard asymptotic methods, it is possible to approximate the above integral for large t as

$$\phi(x,y,z,t)\sim\frac{2F(k,y,z)}{[\omega''(k)t]^{1/2}}\cos\left[kx-\omega(k)t-\frac{\pi}{4}\operatorname{sgn}\omega''(k)\right]\quad(t\to\infty),\tag{4.1}$$

where

$$x/t=\omega'(k_s).\tag{4.2}$$

In interpreting (4.1) we treat x and t as independent variables and regard k [and thus $\omega(k)$] as a function of x/t. Substitution into (2.5a,b) yields

$$\frac{dX}{dt}=U(Y,z)\tag{4.3a}$$

and

$$\frac{dY}{dt}=\frac{\partial}{\partial X}\left\{\frac{2F(k,Y,z)}{[\omega''(k)t]^{1/2}}\cos\left[kX-\omega(k)t-\frac{\pi}{4}\operatorname{sgn}\omega''(k)\right]\right\},\tag{4.3b}$$

where $k=k(X/t)$. In differentiating the right-hand side of (4.3b), note that

$$\frac{dk(X/t)}{dX}=\frac{-k(X/t)X/t}{t},$$

$$=\frac{-k\omega'(k)}{t}\to 0\quad\text{as}\quad t\to\infty.$$

We may thus regard k as constant when performing the x differentiation.

In analyzing the trajectories for a monochromatic wave, it was convenient to transform to a frame of reference moving with the phase speed of the wave in question. It would be less advantageous to do so here since k would be time dependent. Instead let us choose

a particular $k = k_0$ and move at the group velocity $\omega'(k_0)$. Letting

$$X_k = X - \omega'(k_0)t \tag{4.4}$$

and substituting for X in 4.3a and 4.3b, we obtain

$$\frac{dX_k}{dt} = U(Y, z) - \omega'(k_0) \tag{4.5a}$$

$$\frac{dY}{dt} = \frac{-2kF(k, Y, z)}{(\omega''(k)t)^{1/2}} \sin\left\{kX_k - [\omega(k) - k\omega'(k_0)]t - \frac{\pi}{4}\,\mathrm{sgn}\omega''(k)\right\}. \tag{4.5b}$$

The advantage of this transformation is that if we restrict the range of X_k so that k remains nearly constant [$X_k \ll \omega'(k_0)t$], then the functional dependence of k on X/t becomes

$$k(X/t) = k[\omega'(k_0) + X_k/t] = k[\omega'(k_0)] + 0(t^{-1}) \sim k_0 \quad (\text{as } t \to \infty),$$

and we may replace k by k_0 in (4.5b). It is worth remembering that this replacement is valid only over a limited interval of the X_k axis.

An observer in the moving frame sees critical points ($dX_k/dt = 0$, $dY/dt = 0$) determined by

$$U(Y, z) = \omega'(k_{s0}) \tag{4.6}$$

and

$$k_{s0}X_k - [\omega(k_{s0}) - k_{s0}\omega'(k_{s0})]t - \frac{\pi}{4}\,\mathrm{sgn}\omega''(k_{s0}) = 0, \pm\pi, \pm 2\pi, \text{ etc.}$$

At fixed z, the critical points thus lie along the line where the basic velocity equals the group velocity. Let us denote the position of this line $y = y_g$ and call it the "group line." In the moving frame of reference, the critical points occur at intervals of π/k_{s0} along the group line and appear to translate at speed $\omega(k_{s0})/k_{s0} - \omega'(k_{s0})$, the difference between the phase and group speeds.

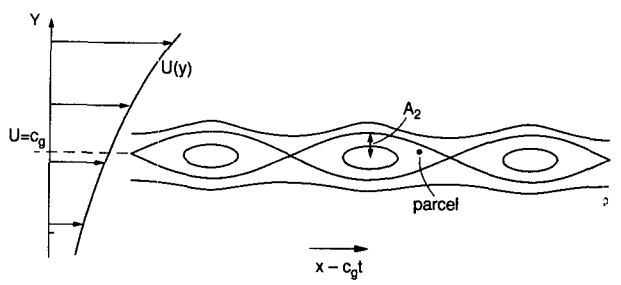

FIG. 11. Moving-frame streakline patterns for a wave packet at about a line $U(y) = c_g$. Initial conditions are given by (4.8) with $k_0 = 1$ and $\omega = 2$.

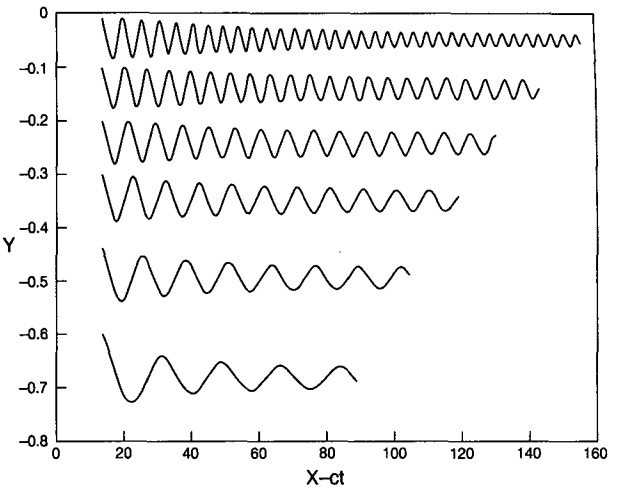

FIG. 12. Fixed-frame trajectories for a raft of floats launched in a dispersing wave packet.

The situation is illustrated in Fig. 11. The streaklines (aligned tangent to parcel motion at a given instant) form the familiar cat's eyes pattern about the group line. The half-width of the cat's eyes (A_2 in Fig. 11) can be estimated using the previous procedure and is found to be

$$A_2 \approx \left[\frac{4F(k_{s0}, y_g, z)}{(dU/dy)_{y=y_g}[\omega''(k_{s0})t]^{1/2}}\right]^{1/2}. \tag{4.7}$$

Care must be exercised in evaluating the role of the cat's eyes, as they are time dependent and do not necessarily imply greater trajectory amplitudes than in other parts of the flow field.

Consider a parcel originating at $t = 0$ in the vicinity of an isolated disturbance and suppose that $Y(0) = y_0$. In a small amplitude wave field the parcel will move in the x direction at a speed approximately equal to $U(y_0, z)$ and may initially execute a complicated sequence of oscillations as different wavenumber pulses of the dispersing disturbance pass by. As time passes, a fixed wavenumber determined approximately by $U(y_0, z) = \omega'(k_0)$ will emerge (should such a k_0 exist), the latitude y_0 will (approximately) become a group line, and the parcel will therefore travel near or within the cat's eyes pattern. Unlike the case for plane waves, the cat's eyes move at 0(1) speed relative to the parcel and decay at rate $t^{-1/4}$ [see (4.7)].

The question now is whether a parcel moving near a group line can execute the irregular trajectories suggestive of mixing that were observed with just two superimposed waves (section 3). Figure 12 shows a raft of trajectories for parcels moving in an isolated disturbance of the cusped jet. [The initial condition is $\phi(x, y, 0) = ae^{-(1+k_0^2)^{1/2}|y|-x^2/\omega^2}\cos k_0 x$, corresponding to

$$F(k, y) = \sqrt{2}awe^{-(1+k^2)^{1/2}|y|-w^2(k-k_0)^2/4}, \quad (4.8)$$

with $k_0 = 1$ and $w = 2$.] The parcels originate at different values of y and move left to right at a speed approximately equal to U at the initial Y. The value of $U(Y(0)) \approx X/t$ determines the approximate wavenumber and frequency of oscillation for each trajectory through the relation (4.2) with $\omega'(k) = 1 - (1 + k^2)^{-3/2}$. Parcels farthest from the jet axis ($y \approx 0$) have the smallest values of x/t and are therefore associated with the lowest k. [The wavenumber of the trajectory is not k but $\omega(k)/U(Y(0))$.]

In the trajectories of Fig. 12, which are plotted over the time interval $20 \leq t \leq 170$, all parcels have ample time to settle into their appropriate wavenumber pulse, as evidenced by the uniformity of the oscillation wavelength within each trajectory. The oscillations also experience the anticipated $t^{-1/4}$ decay. The most striking feature is the complete lack of any irregularity in the trajectories. Thus, it appears that the continuous distribution of wavenumbers expunges behavior suggestive of chaos or mixing, at least in the long-time behavior of our example. It is quite possible that other initial conditions or other basic flows might produce Lagrangian chaos. In the present case, varying the values of w and k_0 over $0.5 < k_0 < 2$ and $1 < w < 4$ does not seem to change the conclusions.

Should a wavenumber k_s exist at which the waves are nondispersive, $\omega'(k_s) = \omega/k$, then the streakline cat's eyes will appear stationary in the moving frame of reference (and, in fact, become trajectories). This situation is much closer to the one that produced irregular trajectories earlier and would be interesting to explore should such a jet exist.

5. Parcel motion due to nonmodal disturbances

The normal modes of the basic flows considered in the previous sections are not complete. In the case of the cusped jet, for example, one could impose an initial condition containing nonzero perturbation potential vorticity. Since the normal-mode perturbation potential vorticity is zero at all points away from the front, the normal modes would be unable to synthesize the disturbance. In order to overcome this difficulty, one must solve the initial-value problem using the prenormal-mode equations. The result of such a calculation is a representation of the solution in terms of normal modes plus a nonmodal component or continuous spectrum. The latter has been used to describe the evolution of highly localized atmospheric disturbances (Ferrell 1987). Recently these ideas have been extended to the ocean setting by Ferrell and Moore (1992) and Moore and Ferrell (1993).

Our purpose here is to isolate the distinctive features of nonmodal parcel trajectories. We attempt to do so by considering the (highly idealized) case of unbounded Couette flow $U = y$, $\beta = 0$, a basic state with no normal modes. The disturbance streamfunction $\phi(x, y, t)$ obeys the prenormal-mode version of (2.1) for barotropic flow:

$$\left(\frac{\partial}{\partial t} + y\frac{\partial}{\partial x}\right)(\phi_{xx} + \phi_{yy}) = 0. \quad (5.1)$$

The general form for the perturbation potential vorticity that obeys (5.1) is

$$q = \phi_{xx} + \phi_{yy} = \mathrm{Re}[q_0 e^{ikx+i(l-kt)y}]. \quad (5.2)$$

An integral over k and l will synthesize an arbitrary initial distribution of potential vorticity. The associated streamfunction is

$$\phi = \mathrm{Re}\left[\frac{-q_0 e^{ikx+i(l-kt)y}}{k^2 + (l - kt)^2}\right]. \quad (5.3)$$

The physical picture is the following. At $t = 0$ the potential vorticity (q) field is sinusoidal in x and y with lines of constant potential vorticity directed perpendicular to the vector $k\mathbf{i} + l\mathbf{j}$. Subsequently, the background shear begins to deform these contours that remain perpendicular to $k\mathbf{i} + (l - kt)\mathbf{j}$. If k and l have the same sign, the contours become meridionally aligned when $t = l/k$. It is at this point that the largest values of meridional velocity ϕ_x occur, as indicated by (5.3). Afterward, the constant q contours are tilted and stretched until they are zonally aligned, and the meridional velocity vanishes.

The opportunity for meridional parcel motion is limited to the early stages of evolution of the flow field, a fact that allows one to put a simple bound on the total meridional excursion. The trajectory equations are

$$\frac{dX}{dt} = Y$$

and

$$\frac{dY}{dt} = \frac{kq_0}{k^2 + (l - kt)^2}\sin[kX + (l - kt)Y]. \quad (5.4)$$

From (5.4) it follows that

$$\begin{aligned} |Y(t) - Y(0)| &\leq \int_0^t |dY/dt|\,dt' \\ &\leq \int_0^t \frac{kq_0\,dt'}{k^2 + (l - kt)^2} \\ &= -q_0 k\left[\tan^{-1}\left(\frac{l}{k} - t\right) - \tan^{-1}\frac{l}{k}\right] \\ &\leq kq_0\left[\tan^{-1}\frac{l}{k} + \frac{\pi}{2}\right] \leq \pi k q_0 \end{aligned}$$

so that

$$|Y(\infty) - Y(0)| \leq \pi k q_0.$$

The bound suggests that large meridional excursions are possible for large disturbances in potential vorticity (large q_0) with fine structure (large k).

Figure 13 shows some groups of trajectories for parcels launched in the eastward part of the flow ($x > 0$). In Fig. 13a ($k = 1$, $l = 100$, $q_0 = 1$), most of the trajectories show eastward drift with one parcel peeling off and entering the westward flow ($x < 0$). (Note that this parcel is *not* the one launched at the southernmost position.) In addition, the parcels generally end up at latitudes different from their launch positions. In Fig. 13b, the amplitude q_0 of the initial potential vorticity disturbance is increased to 10, and the resulting trajectories show larger excursions with some pairs crossing. In Fig. 13c, the same parameters but different launch positions are used, which results in even larger excursions and more crossings being seen. In Fig. 13d, q_0 and l are reduced somewhat, but k is increased. As a result, the excursion bound $\pi k q_0$ is increased from its value 10π in the previous two cases to 30π. Although the bound itself grossly overestimates the actual excursions, an increase in excursions is observed.

The trajectories shown in Fig. 13 all display two distinct characteristics. First, the northward excursions take place monotonically during an isolated transient stage. For large values of l this stage is short lived. Second, the parcels may "mix" in the sense that their latitudinal order of alignment may change.

One caveat should be mentioned: the background potential vorticity gradient in this example is zero, and the presence of such a gradient could reduce the net meridional excursions calculated.

6. Summary and conclusions

Fundamental changes in the geometry of parcel exchange have been found to occur when the meridional structure of a zonal jet is taken into consideration. Instead of enhanced parcel exchange isolated to a steering depth, as with the baroclinic jet studied by LB, parcel exchange is enhanced along a steering surface that lies in the meridional plane. Each horizontal plane of particle motion cuts through the steering surface, leaving isolated steering lines, with the number dependent upon the local geometry of the velocity field. In this paper the characteristics of parcel motion in the vicinity of these steering lines has been examined for the case of linear, neutral waves superposed on a mean zonal jet.

Using kinematic arguments alone, it can be shown that there are two fundamental modes of parcel behavior near steering lines. First, when the local velocity shear is nonzero, a steering line will be characterized by alternating stable and unstable nodes. For the former, particle trajectories orbit a fixed point (in a frame of reference moving with the wave speed) that lies on the steering line. For the latter there are con-

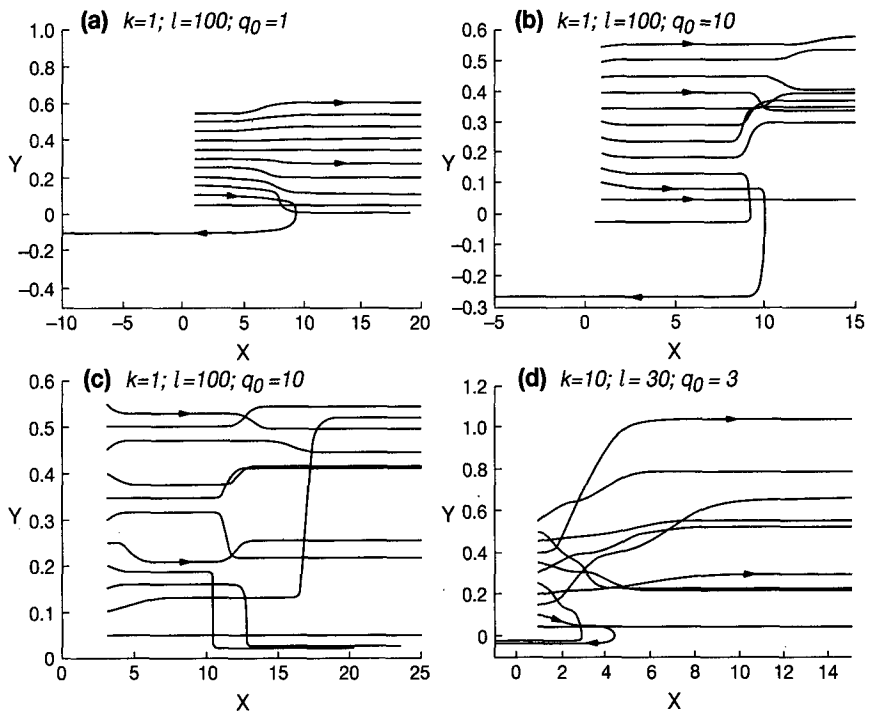

FIG. 13. Fixed-frame trajectories for rafts of floats in a linear shear and in the presence of a nonmodal disturbance. The wavenumbers (k, l) and initial amplitude q_0 of the disturbance are listed.

verging and diverging trajectories associated with a fixed point lying on the steering line. As well documented in chaos theory, the converging and diverging trajectories make the parcel paths sensitive to weak secondary effects, such as diffusion or additional time dependence.

The second mode of parcel behavior occurs when the steering line lies where there is no local meridional velocity shear. In such a case the steering line is either a local maximum in $U - c$ or a local minimum. Thus, relative to the particles at the steering line, all other particles are moving faster (when there is a local minimum) or slower (when there is a local maximum). Therefore, there are no longer any closed orbits and all trajectories are in the same eastward (when there is a local minimum) or westward (when there is a local maximum) direction. This difference in the local geometry of the parcel trajectories means that the convergence of waters from south of the steering line no longer coincides with the convergence of waters from north of the steering line. Thus, even though the relative amplitude of these cusped trajectories is greater than in the case of local shear, the opportunity for exchange across the steering lines is potentially diminished. To the authors' knowledge, a formal theory for chaos (or lack thereof) has not been established for this case.

To examine parcel trajectories in dynamically consistent flow fields, cusped jets with piecewise-uniform meridional potential vorticity structure have been examined. The selected jets support neutral modes with sinuous, varicose, and mixed structure. For the case of local shear, each of these modes shows the same local pattern in the vicinity of the steering lines: cats' eyes alternating with convergent and divergent trajectories. When the steering lines are located where there is no local velocity shear, the sinuous and mixed modes exhibit the same pattern: cusped trajectories approaching the steering lines, with those from the north and the south displaced. From these dynamically consistent flow fields, parcel trajectories were analyzed. For the case of a monochromatic wave, the trajectories are characterized by simple periodic meandering with the wavelength determined by the absolute value of $U - c$. Such regularity does not occur when a second wave is superposed on the zonal jet, in agreement with the previously cited kinematic models. Instead, chaotic trajectories result in the vicinity of the steering line. Although it is tempting to associate a chaotic wave field with strong mixing, we note here that chaotic parcel exchange is not synonymous with dynamical fluxes.

In an effort to test the robustness of the chaotic trajectories that resulted from the two-wave perturbation, a Fourier superposition of neutral waves was imposed on a zonal jet. Surprisingly, in the long time limit the trajectories from such a superposition were marked by nearly periodic meandering. There was no visual trace of irregularity. For the initial condition and jet used, the continuous distribution of waves curtails the chaotic behavior found in the two-wave case. Mixing in such a system may be relegated to the initial stages after the disturbance. These results warrant a further exploration of other jets and initial conditions for generalization.

A further generalization, that of including nonmodal perturbations, reinforces the notion that mixing is enhanced in the early stages after a disturbance, because for this case all meridional velocities vanish over time. In an effort to isolate nonmodal contributions to the parcel paths, a simple Couette flow was used. Excursions were found to be large in the early stages for large potential vorticity perturbations and small wavelengths. The nature of the excursions is such that parcels can change their cross-stream positions, thus implying a significant potential for mixing. Again, these results should be reexamined under more general background potential vorticity distributions.

The major result of this work, that parcel exchange is enhanced at selected sites along a horizontal plane of motion, implies that mixing within a jet, such as the Gulf Stream, is not restricted to a single depth, but rather occurs over a range of depths. For a typical Gulf Stream velocity profile and for a typical Gulf Stream phase speed, mixing would be at the edges in the upper waters and would move toward the center of the stream as depth increased. Such a scenario would be consistent with interleavings found at the edges of the upper Gulf Stream (Lillibridge et al. 1990) and homogenization of water properties found at the center of the stream for the middepths (Bower et al. 1985).

For the jets studied here a wavenumber can be found such that each meridional position is a steering line, except for the latitude demarcating the potential vorticity front. It has been shown that for a neutral wave to exist, a steering line must coincide with a region where there is no potential vorticity gradient. For the piecewise uniform jets of this study, this is not restrictive except for excluding the front itself. Considering a jet with continuous meridional potential vorticity structure, however, the choices of possible steering lines are quite limited. Taking this a step further to a case of a baroclinic jet, a steering surface must coincide with an isotach. Although this can be achieved by choosing a suitable velocity field, such a requirement in general essentially precludes the existence of neutral modes with steering lines and thus implies limited mixing. To circumvent this exclusion, one can argue for potential vorticity homogenization along a steering surface or appeal to the unstable modes of the system. The latter approach will be chosen for the major extension of this work, which is to examine parcel behavior within a jet marked by a continuous background potential vorticity gradient. With this extension we aim to determine how parcel pathways are affected by the dynamic constraint of potential vorticity conservation.

Acknowledgments. This work was supported by the Office of Naval Research under Contract N00014-89-

J-1182. We thank Deborah Taylor for preparing the manuscript and the anonymous reviewers for their constructive comments.

REFERENCES

Behringer, R. P., S. D. Meyers, and H. L. Swinney, 1991: Chaos and mixing in a geostrophic flow. *Phys. Fluids A.*, **3**, 1243–1249.

Bower, A. S., 1991: A simple kinematic mechanism for mixing fluid parcels across a meandering jet. *J. Phys. Oceanogr.*, **21**, 173–180.

——, and T. Rossby, 1989: Evidence of cross-frontal exchange processes in the Gulf Stream based on isopycnal RAFOS float data. *J. Phys. Oceanogr.*, **19**, 1177–1190.

——, and M. S. Lozier, 1994: A closer look at particle exchange in the Gulf Stream. *J. Phys. Oceanogr.*, **24**, 1399–1418.

——, H. T. Rossby, and J. L. Lillibridge, 1985: The Gulf Stream—barrier or blender? *J. Phys. Oceanogr.*, **15**, 24–32.

Charney, J. G., and M. Stern, 1962: On the stability of interval baroclinic jets in a rotating atmosphere. *J. Atmos. Sci.*, **19**, 159–172.

Cushman-Roisin, B., 1993: Trajectories in Gulf Stream meanders. *J. Geophys. Res.*, **98**, 2543–2554.

del-Castillo-Negrete, D., and P. J. Morrison, 1993: Chaotic transport by Rossby waves in shear flow. *Phys. Fluids A.*, **5**, 948–965.

Dutkiewicz, S., A. Griffa, and D. B. Olson, 1993: Turbulent diffusion in a meandering jet. *J. Geophys. Res.*, **98**, 16 487–16 500.

Ferrell, B. F., 1987: Developing disturbances in shear. *J. Atmos. Sci.*, **44**, 2191–2199.

——, and A. E. Moore, 1992: An adjoint method for obtaining the most rapidly growing perturbation to oceanic flows. *J. Phys. Oceanogr.*, **22**, 338–349.

Garvine, R. W., 1988: Flow field properties of long, propagating frontal waves. *J. Phys. Oceanogr.*, **18**, 788–792.

Haynes, P. H., 1989: The effect of barotropic instability on the nonlinear evolution of a Rossby wave critical layer. *J. Fluid Mech.*, **207**, 231–266.

——, and M. E. McIntrye, 1987: On the representation of Rossby-wave critical layers and wave breaking in zonally truncated models. *J. Atmos. Sci.*, **44**, 2359–2382.

Lillibridge, J. L., G. Hitchcock, T. Rossby, E. Lessard, M. Mork, and L. Golmen, 1990: Entrainment and mixing of shelf/slope waters in the near-surface Gulf Stream. *J. Geophys. Res.*, **95**, 13 065–13 087.

Lozier, M. S., and S. C. Riser, 1990: Potential vorticity sources and sinks in a quasigeostrophic ocean: Beyond western boundary currents. *J. Phys. Oceanogr.*, **20**, 1608–1627.

——, and D. Bercovici, 1992: Particle exchange in an unstable jet. *J. Phys. Oceanogr.*, **22**, 1506–1516.

Moore, A. E., and B. F. Ferrell, 1993: Rapid perturbation growth on spatially and temporally varying ocean flows determined using an adjoint method: Application to the Gulf Stream. *J. Phys. Oceanogr.*, **23**, 1682–1702.

Pedlosky, J., 1979: *Geophysical Fluid Dynamics.* Springer-Verlag, 624 pp.

Polvani, L. M., and J. Wisdom, 1990: Chaotic Lagrangian trajectories around an elliptical vortex patch embedded in a constant and uniform background shear flow. *Phys. Fluids*, **A2**(2), 123–126.

Pratt, L. J., and M. E. Stern, 1986: Dynamics of potential vorticity fronts and eddy detachment. *J. Phys. Oceanogr.*, **16**, 1101–1120.

——, J. Earles, P. Cornillon, and J.-F. Cayula, 1991: The nonlinear behavior of varicose disturbances in a simple model of the Gulf Stream. *Deep-Sea Res.*, **32**(Suppl. 1), S591–S622.

Samelson, R. M., 1992: Fluid exchange across a meandering jet. *J. Phys. Oceanogr.*, **22**, 431–440.

Sommeria, J., S. D. Meyers, and H. L. Swinney, 1989: Laboratory model of a planetary eastward jet. *Nature*, **337**, 58–61.

Yang, H., 1991: Wave packets and their bifurcations in geophysical fluid dynamics. *Appl. Math. Sci.*, **85**, Springer-Verlag, 247 pp.